Reg Environ Change
DOI 10.1007/s10113-014-0725-6

ORIGINAL ARTICLE

Critical elevation levels for flooding due to sea-level rise in Hawai‘i

Haunani H. Kane · Charles H. Fletcher · L. Neil Frazer · Matthew M. Barbee

Received: 6 September 2013 / Accepted: 6 November 2014

Abstract Coastal strand and wetland habitats in the Hawaiian Islands are often intensively managed to restore and maintain biodiversity. Due to the low gradient of most coastal plain environments, the rate and aerial extent of sea-level rise (SLR) impact will rapidly accelerate once the height of the sea surface exceeds a critical elevation. Here, we develop this concept by calculating a SLR critical elevation and joint uncertainty that distinguishes between slow and rapid phases of flooding. We apply the methodology to three coastal wetlands on the Hawaiian Islands of Maui and O‘ahu to exemplify the applicability of this methodology for wetlands in the Pacific island region. Using high-resolution LiDAR digital elevation models, flooded areas are mapped and ranked from high (80 %) to low (2.5 %) risk based upon the percent probability of flooding under the B1, A2, and A1Fl emissions scenarios. As the rate of flooding transitioned from the slow to rapid phase, the area (expressed as a percentage of the total) at a high risk of flooding under the A1Fl scenario increased from 21.0 to 53.3 % (south Maui), 0.3 to 18.2 % (north Maui), and 1.7 to 15.9 % (north O‘ahu). At the same time, low risk areas increased from 34.1 to 80.2, 17.7 to 46.9, and 15.4 to 46.3 %. The critical elevation of SLR may have already passed (2003) on south Maui, and decision makers on North Maui and O‘ahu may have approximately 37 years (2050) to develop, and implement adaptation strategies that meet the challenges of SLR in advance of the largest impacts.

Keywords Sea-level rise · Wetland · Critical elevation · LiDAR · Digital elevation model · Hawaii

Editor: Virginia R. Burkett.

Electronic supplementary material The online version of this article (doi:10.1007/s10113-014-0725-6) contains supplementary material, which is available to authorized users.

H. H. Kane (✉) · C. H. Fletcher · L. N. Frazer · M. M. Barbee
SOEST/Geology and Geophysics, University of Hawai‘i,
1680 East West Road, Honolulu, HI 96822, USA
e-mail: hkane@hawaii.edu

C. H. Fletcher
e-mail: fletcher@soest.hawaii.edu

L. N. Frazer
e-mail: neil@soest.hawaii.edu

M. M. Barbee
e-mail: mbarbee@soest.hawaii.edu

Introduction

Few studies have examined the consequences of sea-level rise (SLR) on the biodiversity of low-elevation island ecosystems (Reynolds et al. 2012). In the Pacific region alone, over 2,500 islands and atolls harbor a diverse range of freshwater, coastal, and marine wetlands (Ellison 2009). Increased water levels, erosion, salinity, and flooding associated with SLR threaten habitats of endangered waterbirds, sea turtles, monk seals, and migratory shorebirds. In addition, many small coastal marshes are used for subsistence and commercial fishing as well as taro (*Colocasia esculenta*) agriculture.

For most coastal plain environments, the rate of impact due to SLR flooding will rapidly accelerate once the height of the sea surface exceeds a critical elevation. Using a hypsometric model (Zhang 2011; Zhang et al. 2011), we identify the critical elevation marking the end of slow flooding and the onset of rapid flooding. Mapping each phase of flooding and establishing the chronology of impacts provides wetland decision makers with valuable

Published online: 29 November 2014

information about the height of sea-level that poses the greatest threat and the timeframe for which the bulk of wetland assets may be threatened.

The objective of this study is to develop a methodology that identifies the onset of the greatest impacts related to SLR. Our results provide a physical process-based planning horizon useful for decision makers who are developing management strategies to meet the challenges of climate change. This approach will allow future generations to form flexible adaptation management plans based on prioritized (and changing) habitat needs as sea-level rises.

Mapping SLR vulnerability

One way of communicating the risk of SLR is to map low-lying areas using high-resolution light detection and ranging (LiDAR) digital elevation models (DEMs). SLR inundation maps are created by "flooding" those raster DEM cells that have an elevation at or below a given modeled sea surface height (Gesch 2009). Previous studies have considered only marine sources of inundation by mapping DEM cells that are hydrologically connected to the ocean through a continuous path of adjacent flooded cells (Gesch 2009; Poulter and Haplin 2008). Here, we consider both marine and groundwater inundation types (Cooper et al. 2013a) because marine inundation alone underestimates SLR impacts (Rotzoll and Fletcher 2012) and does not account for rising groundwater tables (Bjerklie et al. 2012). This is a reasonable assumption as water table elevations in coastal settings sit typically above mean sea-level (MSL) and are highly correlated with daily tides and other sources of marine energy (Hunt and De Carlo 2000; Rotzoll et al. 2008; Rotzoll and Fletcher 2012). In addition, many managed wetlands are dependent upon natural or pumped groundwater sources to maintain pond water levels (DLNR 2002; Hunt and De Carlo 2000; U.S. Fish and Wildlife Service 2011a, b).

SLR models

Sea-level at any location depends upon a number of different factors including vertical land stability, changes in Earth's gravitational field and spin, variations in steric SLR, fluctuations in winds and currents, and others (Spada et al. 2013). By the year 2100, the equatorial Pacific is projected to reach sea-level values between 10 and 20 % above the global mean (IPCC 2013). The occurrence of temporary extreme high water events is very likely to increase in this region and could intensify SLR impacts. The greatest increases in sea-level (up to 30 % above the global mean) are projected in the Southern Ocean and the eastern coast of North America and are related to changes in wind forcing, circulation and the redistribution of heat and freshwater. The greatest decreases in sea-level (50 % the global mean) are predicted for the Arctic region and some regions near Antarctica (IPCC 2013) because as land ice melts, its gravitational attraction of ocean water weakens and results in decreasing sea-level near the ice.

We apply global SLR rates to Hawai'i because regional models fail to capture observed local weather patterns, local subsidence, produce inconsistencies among projections (Tebaldi et al. 2012), and map SLR for only one point in time. A number of global SLR estimates have been created for the year 2100 and beyond using physics-based approaches (e.g., Slangen et al. 2012), semi-empirical methods (e.g., Schaeffer et al. 2012), and expert judgment assessment (e.g., Bamber and Aspinall 2013). Semi-empirical and expert judgment methods provide alternatives to physical models because dynamic systems such as ice sheets are not fully understood (IPCC 2007; IPCC 2013; Vermeer et al. 2012). In particular, the semi-empirical method of Vermeer and Rahmstorf (2009) offers a unique solution for the position of future sea-levels by providing MSL curves and associated uncertainty (1σ) bands across the 19 climate models used in the Intergovernmental Panel on Climate Change (IPCC) fourth assessment report (AR4) (2007). In addition, this model provides multiple emission scenarios to address how future global sea-level may change under different social, economic, technological, and environmental developments (IPCC 2000). The robustness of Vermeer and Rahmstorf's (2009) projections of future SLR has been well documented by Rahmstorf et al. (2011).

Due to the lack of a regional SLR model for Hawai'i and the recent release of the IPCC's AR5 projections in comparison with the timeline of this project we apply Vermeer and Rahmstorfs (2009) global SLR scenarios to assess the impacts of SLR flooding upon Pacific Island coastal ecosystems. The SLR curves provided by this model enable decision makers to correlate impacts of slow and rapid phases of flooding with a sea-level height and time. We encourage managers to plan for three scenarios of future sea-level. The B1 (1.04 m by 2100), A2 (1.24 m), and A1FI (1.43 m) scenarios encompass the range of SLR projections forecasted by regional models (e.g., Spada et al. 2013) for the Central Pacific by the end of the century. The methodology used here is applicable to not only Hawai'i but all Pacific Island coastal ecosystems. The methodology may be updated with new SLR models as global and regional projections improve.

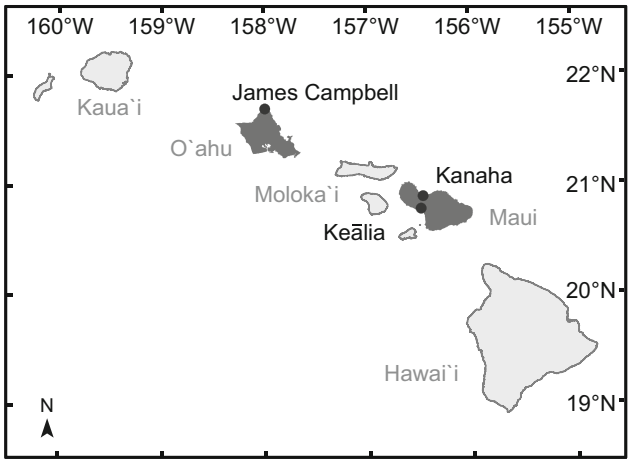

Fig. 1 Wetland study area on the north and south shores of the islands of Maui and O'ahu, Hawai'i

Methods

Study area

To address the problem of nonlinear inundation, we study three coastal wetlands in Hawai'i: (1) James Campbell National Wildlife Refuge (north O'ahu), (2) Kanaha Pond State Wildlife Sanctuary (north Maui), and (3) Keālia Pond National Wildlife Refuge (south Maui) (Fig. 1). All three wetlands are intensively managed by either the Fish and Wildlife Service (FWS) or the Hawai'i State Department of Land and Natural Resources (DLNR). One of the main state and federal management priorities of Hawaiian wetlands is to restore and maintain self-sustaining populations of endangered waterbirds including the Hawaiian Coot (*Fulica alai*), Hawaiian Moorhen (*Gallinula chloropus sandvicensis*), Hawaiian Stilt (*Himantopus mexicanus knudseni*), and the Hawaiian duck (*Anas wyvilliana*) (U.S. Fish and Wildlife Service 2011c). Three of the four most frequently observed plant species are exotic and highly invasive; California grass (*Urochloa mutica*), pickleweed (*Batis maritime*), and seashore paspalum (*Paspalum vaginatum*). The dominant native species is water hyssop (*Bacopa monnieri*) (Bantilan-Smith et al. 2009). Springs, rainfall, and runoff feed these wetlands, however, during the dry season managers may supplement pond water levels with additional sources of groundwater. Hawai'i's coastal wetlands are microtidal (maximum tidal range of 0.91–1.12 m on O'ahu and Maui, respectively) (accessed at http://tidesandcurrents.noaa.gov/noaatidepredictions/), largely isolated from the ocean, and sediment sources include eolian dust, intermittent stream flooding during the wet season (October–April), and internally produced organic solids (U.S. Fish and Wildlife Service 2011a). Poorly drained and moderately to strongly saline hydric soil types were identified in each study area using soil maps derived from the Natural Resource Conservation Service (NRCS) web soil survey (accessed at http://websoilsurvey.nrcs.usda.gov/app/). Dominant hydric soils include Kealia silt loam, Kaloko clay, Keaau clay, and Pearl Harbor clay.

With the exception of narrow ocean outlet ditches, all three coastal wetland study sites are buffered from marine impacts by a narrow coastal strand. In this study, the coastal strand encompasses the beach, 2–4 m sand dunes and the zone immediately inland of the dunes (U.S. Fish and Wildlife Service 2011a). Depending upon the coastal strand for critical habitat is native plants, the endangered Hawaiian monk seal (*Monachus schauinslandi*), the threatened Hawaiian green sea turtle (*Cheloniamydas*), and migrant shorebirds during winter months.

Data processing

Two separate datasets were used for our three study areas. The data for Keālia were collected in 2006 by Airborne 1, a LiDAR services company contracted by the Federal Emergency Management Agency (FEMA). FEMA reports an average point spacing close to 0.30 m and a $RMSE_z$ of 0.18 m (Dewberry 2008). The data for James Campbell and Kanaha were collected during January and February 2007 by the Joint Airborne LiDAR Bathymetry Technical Center of Expertise (JABLTCX) for the U.S. Army Corps of Engineers (USACE). USACE metadata reports an average point spacing of 1.3 m and a vertical accuracy of better than ± 0.20 m (1σ). For the purpose of this study, we assume the $RMSE_z$ and 1σ are equivalent (NOAA 2010).

Both data sets were collected in geographic coordinates and ellipsoid heights relative to the North American Datum of 1983 (NAD83). The true surface of the earth however varies slightly from the smooth surface of an ellipsoid; therefore, ellipsoid elevations were transformed to orthometric elevations using the Geoid03 model. Geoid models are equipotential surfaces defined by Earth's gravity field, and the zero contour of a geoid model approximates the global MSL shoreline (Cooper et al. 2013b). These elevations were then adjusted to the Local Tidal Datum of MSL based upon a 2006 epoch for the USACE dataset and a 2002 epoch for the FEMA dataset. It is important to note that the differences in epoch values in Hawai'i are small when compared to the other contributions to the vertical accuracy of the LiDAR data. Last return features,or bare earth LiDAR were converted from LAS format to ESRI shapefile format and were reprojected to Universal Transverse Mercator (UTM) zone 4 North.

Triangular irregular networks (TIN) were derived from the processed and filtered LiDAR point data for each study area. To identify areas where point density poorly characterizes coastal morphology, a distance of 20 m

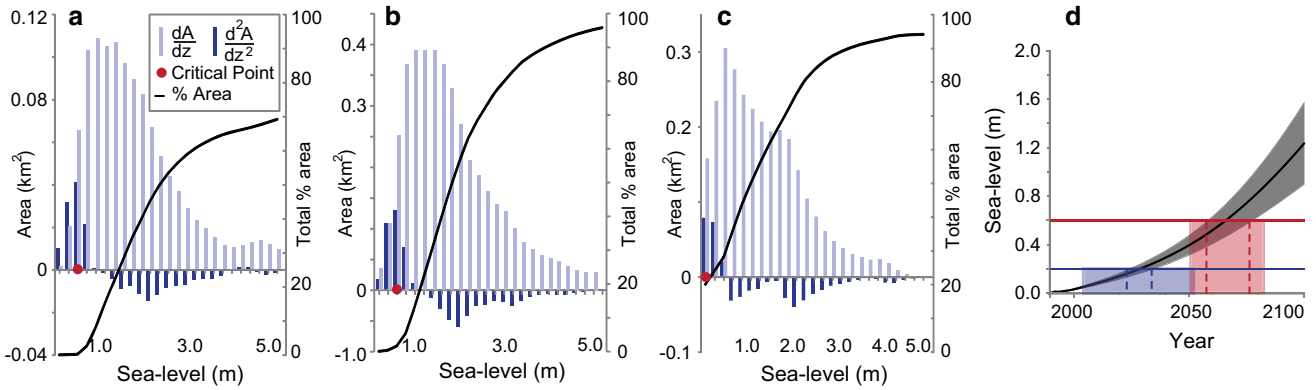

Fig. 2 Land area hypsometric curves at **a** Kanaha, **b** James Campbell, and **c** Keālia. The *x*-axis represents elevation (m) above MHHW. The *y*-axes represent total percent area at or below a corresponding sea-level value, and area (km^2) inundated as sea-level rises in 0.2 m increments. Temporal uncertainty of the critical elevation is depicted in (**d**), based upon the uncertainty of SLR projections alone (*dashed lines*) and the joint uncertainty of SLR projections and topography (*shaded region*)

(maximum edge length) was used to constrain the TIN extents. A 2 m horizontal resolution DEM was interpolated from each TIN using the nearest neighbor method to represent the corresponding bare earth topography.

Critical elevation

We use a land area hypsometric curve (Zhang 2011; Zhang et al. 2011) to identify a critical elevation and characterize the rate of flooding based upon local topography (Fig. 2). We adhere closely to NOAA Coastal Services Center Coastal Inundation Toolkit Mapping Methodology (accessed at http://www.csc.noaa.gov/slr/viewer/assets/pdfs/Inundation_Methods.pdf) and use DEMs to model the area flooded as sea-level is increased from 0 to 5.0 m.

Following the methodology of Cooper et al. (2013b) and due to the lack of a North American Vertical Datum of 1988 (NAVD 88) for Hawai'i, we map MSL values upon the 19-year epoch value of mean higher high water (MHHW) at the Honolulu tide gauge for James Campbell and at the Kahului tide gauge for Kanaha and Keālia to assess flooding at high tide (accessed at tidesandcurrents.noaa.gov). The hypsometric curve depicts the additional area that is flooded (dA) as sea-level is increased in increments of 0.20 m, which approximates the LiDAR vertical uncertainty. We calculated the rate (dA/dz) and acceleration (d^2A/dz^2) of flooding with respect to elevation (z). This approach depicts a generalized view of flooding impacts dependent solely upon the local topography of a study area.

The critical elevation is identified at the sea-level at which d^2A/dz^2 is a maximum. Managers find it useful to not only plan for a critical elevation, but also the timeframe in which the critical elevation may be exceeded. Combined with the SLR projection gives the speed (dA/dt) and acceleration of flooding (d^2A/dt^2). For a linear rise in sea-level with time, the critical elevation separates flooding into a slow phase (relatively low dA/dt) and a fast phase (relatively high dA/dt). To determine the temporal uncertainty of each flooding phase, we create a mixture distribution SLR curve from Vermeer and Rahmstorf's (2009) B1, A2, and A1FI SLR curves. The B1 (1.04 m by 2100), A2 (1.24 m), and A1FI (1.43 m) emission scenarios address how future global sea-level may change under different social, economic, technological, and environmental development pathways (IPCC 2007). Because the probability of occurrence for each SLR scenario is unknown, we first generalize the critical elevation across all three scenarios. Assuming each scenario SLR curve is evenly weighted and normally distributed, we calculate the total mean ($\mu(t)$) and variance ($\sigma^2(t)$) of the final SLR curve, respectively:

$$\mu(t) = \frac{1}{3}\mu_{\mathrm{B1}}(t) + \frac{1}{3}\mu_{\mathrm{A2}}(t) + \frac{1}{3}\mu_{\mathrm{A1FI}}(t) \tag{1}$$

$$\sigma^2(t) = \frac{1}{3}\left[(\mu_{\mathrm{B1}} - \mu(t))^2 + \sigma^2_{\mathrm{B1}}\right] + \frac{1}{3}\left[(\mu_{\mathrm{A2}} - \mu(t))^2 + \sigma^2_{\mathrm{A2}}\right] + \frac{1}{3}\left[(\mu_{\mathrm{A1FI}} - \mu(t))^2 + \sigma^2_{\mathrm{A1FI}}\right] \tag{2}$$

From the SLR curve we calculate the temporal uncertainty of the critical elevation based upon SLR projections alone (σ_{t_s}) and SLR projections and topography ($\sigma_{t_{s+z}}$). This analysis allows us to determine whether incorporating hypsometry into management and planning makes a quantifiable difference.

$$\sigma_{t_s} = \frac{\sigma_s(t_T)}{\frac{d\mu_s(t_T)}{dt}} \tag{3}$$

$$\sigma_{t_{s+z}} = \frac{\sqrt{\sigma_s(t_T)^2 + \sigma_z(t_T)^2}}{\frac{d\mu_s(t_T)}{dt}} \quad (4)$$

Mapping the risk of flooding

We account for the uncertainty of SLR projections and LiDAR data in our SLR flood maps using a combination of several existing standards. A cumulative percent probability approach is used to define the risk (or probability) of flooding. We map areas of high (80–100 % probability), moderate (50–100 % probability), and low (2.5–100 % probability) risk. The 80 % probability contour identifies high confidence flood areas (NOAA 2010), while the 50 % rank maps the area flooded by the predicted sea-level value alone. Gesch (2009) and the National Standard for Spatial Data Accuracy (FGDC 1998) recommended the use of the linear error at the 95 % confidence level (1.96 × $RMSE_z$) to identify additional areas that may be inundated at time t. The 2.5 % rank used in this study to identify low risk areas equates to a standard score of 1.96 when a cumulative or single tail approach is used (NOAA 2010).

To assess the percent probability that a location (x, y) will be inundated at time t, we adhere closely to NOAA (2010) and Mitsova et al. (2012). For each economic scenario, a 2 m horizontal resolution raster is created to calculate the expected height above MHHW (μ_h) at time t. We take the difference between the projected sea-level value above MHHW (μ_s) and the DEM elevation (μ_z):

$$\mu_h = \mu_s - \mu_z \quad (5)$$

To account for the uncertainty (σ_t) associated with an area's expected height above MHHW, we combine two random and uncorrelated sources using summing in quadrature (Fletcher et al. 2003): SLR model uncertainty (σ_s) and LiDAR vertical uncertainty (σ_z).

$$\sigma_t = \sqrt{\sigma_s^2 + \sigma_z^2} \quad (6)$$

The SLR model uncertainty reflects a semi-empirical characterization of the physical link between climate change and SLR, and the LiDAR uncertainty is a measure of the vertical accuracy of the LiDAR points to represent the corresponding bare earth topography. A second surface is created to represent the standard score (SS_{XY}) or the number of standard deviations a value falls from the mean.

$$SS_{XY} = \frac{\mu_h}{\sigma_t} \quad (7)$$

The standard score raster is reclassified to a percent probability raster by means of a look up table assuming normally distributed errors. Under each phase of SLR, we map and calculate the percent area with low, moderate, and high risk of flooding for the B1, A2, and A1FI scenarios. Reengineered areas such as the diked ponds at James Campbell are not included in this analysis.

Results and discussion

Defining a critical elevation

We identify a critical elevation that separates flooding into a slow and fast phase based upon the local topography of three coastal wetlands. The critical elevation of Keālia is defined at 0.2 m and is predicted to be exceeded by the year 2028 ± 25 years (Fig. 2). Kanaha and James Campbell study areas are located at a slightly higher elevation resulting in a critical elevation of 0.6 m by 2066 ± 16 years. Currently, approximately 0.1 % of James Campbell, 20.1 % of Keālia, and 0.1 % of Kanaha are found at or below an elevation equivalent to MHHW.

We acknowledge that the time frame of exceedance for the critical elevation is quite large and is mostly a reflection of the quality of currently available data. To determine the critical elevation, we deal with two sources of uncertainty; the uncertainty of the SLR model used to correlate sea-level with time and the uncertainty of the LiDAR data used to identify and map the critical elevation. The large LiDAR uncertainty proves to be a major limiting factor. In comparison with considering SLR model uncertainty alone, accounting for the joint uncertainty of both datasets increases the temporal component of the critical elevation from ±5 to ±25 years at Keālia and ±9 to ±16 years at James Campbell and Kanaha. As SLR projections and topographic datasets improve, the methods used in this study can be employed with greater confidence.

Mapping SLR impacts for slow and fast phases of flooding

Here, we find the slow phase of flooding is defined from present to 2028 ± 25 years (critical elevation = 0.2 m) at Keālia and from present to 2066 ± 16 years (0.6 m) at Kanaha and James Campbell (Fig. 3, supplementary Figures 1, 2). To assist decision makers in prioritizing SLR impacts, we map flooded areas of high, moderate, and low risk. Due to the similarity of SLR curves during the slow phase, all three emission scenarios agree that there is a moderate risk of 24.1 % of Keālia, 2.8 % of Kanaha, and 4.3 % of James Campbell being flooded (Table 1). High and low risk areas encompass 21.0–34.1 % of Keālia, respectively, 0.3–17.7 % of Kanaha, and 1.7–15.4 % of James Campbell. The slow phase of flooding represents the onset of vulnerability as SLR increases coastal erosion and the extent and frequency of storm surges. Although initial

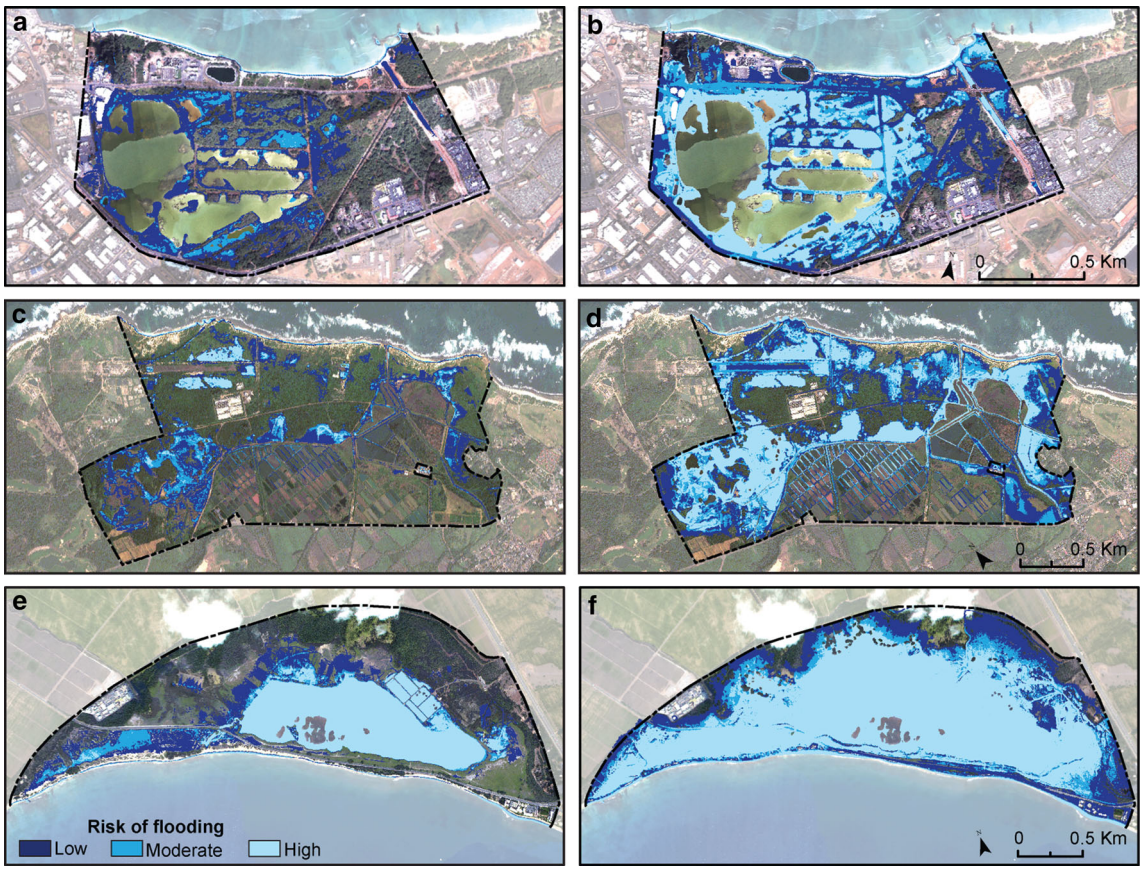

Fig. 3 A1FI SLR risk comparison for slow (left column images) and fast phases of flooding at **a**, **b** Kanaha, **c**, **d** James Campbell, and **e**, **f** Keālia

Table 1 Percent area of land vulnerable to high, low, and moderate risk for the slow and fast phase of flooding

Study area	Flooding phase	Scenario	% Area		
			High risk	Moderate risk	Low risk
James Campbell	Slow	B1, A2, A1FI	1.7	4.3	15.4
	Fast	B1	7.6	14.3	33.5
		A2	14.3	19.9	40.5
		A1FI	15.9	25.9	46.3
Kanaha	Slow	B1, A2, A1FI	0.3	2.8	17.7
	Fast	B1	7.0	16.4	36.2
		A2	13.2	22.6	43.2
		A1FI	18.2	28.8	49.6
Keālia	Slow	B1, A2, A1FI	21.0	24.1	34.1
	Fast	B1	42.7	51.3	67.6
		A2	48.5	57.0	74.1
		A1FI	53.3	62.2	80.2

percent area impacts may appear small, threatened areas include majority of the coastline and inland wetland environments at James Campbell and Keālia (Fig. 3).

The fast phase of flooding represents a time in which the bulk of impacts due to SLR is predicted to occur. We define the fast phase of flooding from 2028 ± 25 years to 2100 at Keālia and 2066 ± 16 years to 2100 at Kanaha and James Campbell. These results indicate that the critical elevation of SLR may have already passed (2003) on south Maui, and that decision makers may have approximately 37 years (2050) on North Maui and O‘ahu to conceive, develop, and implement adaptation strategies that meet the challenges of SLR in advance of the largest impacts.

We do not consider the post-21st century extent of the fast phase as indicated by the hypsometric curve because our SLR model does not exceed the year 2100. At 1.04 m (B1) of SLR, there is moderate risk of flooding for 51.3 % of Keālia, 16.4 % of Kanaha, and 14.3 % of James Campbell. At 1.24 m (A2), moderate risk SLR impacts increase to 57 % of Keālia, 22.6 % of Kanaha, and 19.9 % of James Campbell. Under the worst case scenario of 1.43

(A1FI), moderate risk of flooding impacts increase to 62.2 % of Keālia, 28.8 % of Kanaha, and 25.9 % of James Campbell. SLR impacts experienced along the beaches during the slow phase expand and encroach into the upland vegetation and inland wetlands during the fast phase of flooding. At all three study areas, nearly all of the wetlands are subjected to moderate or low risk of flooding.

Strategies to manage SLR impacts

Hawai'i's coastal wetlands are representative of Pacific Island wetlands due to their relatively small size, diversity of endemic and endangered species, and proximity to rapidly increasing human populations that depend upon wetland resources. Impacts associated with SLR exacerbate flooding of nearby coastal communities during storm events, as well as habitat loss, which is widely used as a measurement of the risk of extinction (Iwamura et al. 2013). Globally, resource managers will be challenged to preserve existing habitats through engineering, relocating habitats to higher elevations, and abandoning existing habitats when the magnitude of SLR overwhelms all other efforts.

Using the inundation maps provided in this study, wetland managers can begin prioritizing responses for the slow and rapid phases of SLR flooding. Providing a local critical elevation and a timeframe for the largest impacts of SLR enables wetland managers to begin formulating long-term adaptive management strategies beyond the mandated 15 year planning timeframe that is currently used by Hawai'i wetland managers. The methods used here are applied to wetlands in Hawai'i; however, they are applicable to all coastal stakeholders interested in managing resources and defining new policies in response to SLR.

Management efforts for the slow phase of flooding should be focused primarily on moderate and high risk of flooding areas at the beaches and coastal strand. SLR is an important factor in historical shoreline change (Romine et al. 2013), and future SLR will likely worsen the long-term coastal erosion rates (Fletcher et al. 2013; Zhang et al. 2004). The first organisms to be impacted by SLR include the endangered monk seals that require beaches for resting and molting (Baker et al. 2006) and the sea turtles that require beaches for nesting (Fuentes and Cinner 2010). Intertidal habitats also serve as important staging sites where migrant shorebirds can feed and rest and the loss of such sites can cause severe 'bottleneck' effects on migratory populations (Iwamura et al. 2013). As sea-level continues to rise, beaches will naturally migrate landwards unless prevented by structures such as roads, home lots. (Fish et al. 2008). Facilitating the cross-shore movement of beach habitats may preserve endangered and threatened organisms.

During the slow phase of flooding, wetland managers will need to begin creating an inventory of management priorities to create the capacity to manage accelerated impacts during the fast phase of flooding. As SLR transitions into the fast phase, flooding along the beaches will begin to encroach landward as both marine and groundwater elevations rise. Wetland managers at the three study sites recommend the implementation of water control structures and permanent pumps in areas that are predicted to experience permanent flooding. In addition, increased salinity may cause habitat change as salt tolerant vegetation replaces the native plants required by waterbirds for food, foraging, and the construction of nests.

The timeframe by which intensive management can aid in the preservation of coastal habitats is limited. Wetland mitigation sites will need to be identified both within and potentially outside of current wetland refuge boundaries. For example, upland habitats will need to be opened and cleared to create new nesting sites for the endangered Hawaiian stilt, which is extremely sensitive to increased water levels. Making these decisions, in the context of specific timeframes of vulnerability, may enhance the capacity of stakeholders to create management plans that increase the resiliency of systems and support the ability of natural systems to adapt to change.

This study is one of the first of its kind to attempt to model SLR impacts for Hawaiian wetlands. The next logical step is to expand the definition of wetland risk to include the physical and biological processes that enable coastal wetlands to adjust to SLR. Recent studies centered upon mangrove forest in Micronesian high islands have found that the mangrove environments have a strong capacity to offset elevation losses by way of sedimentation (Krauss et al. 2003, 2010). A second study found that Micronesian mesei or taro fields (a form of a manmade wetland) have the ability to trap up to 90 % of land based sediments (Koshiba et al. 2013). Currently, there are no studies on the sedimentation rates in Hawaiian wetlands.

It has been argued that a more effective approach to evaluate specific wetland vulnerability to SLR is to couple high-resolution spatial data sets like the ones used in this study with precise point-based measurements of wetland vertical accretion. The rod surface elevation table-marker horizon is the primary technique used to measure the vertical movement of the coastal wetlands surface. The surface elevation table is a benchmark rod that is driven through the soil profile (approximately 10–25 m) and equipped with a horizontal arm to measure the distance to the substrate surface from a specified elevation (Webb et al. 2013). The surface elevation table is usually accompanied by artificial marker horizons made of feldspar or sand to monitor surface elevation change. By improving our knowledge of wetland surface and subsurface

processes, we may better understand how Hawaiian wetlands will respond to SLR.

Conclusion

Characterizing flooding into slow and fast phases provides decision makers with a locally based time frame to implement plans to manage the largest impacts of SLR. As time progresses and the fast phase of flooding approaches, the risk associated with delayed decision-making increases. The SLR vulnerability maps created in this study can be used as a guide to identify threatened areas and initiate decision-making that benefits both wetland and coastal strand environments and the neighboring community. By assessing the joint uncertainty of both datasets used in this study, wetland managers can refine their definition of threatened areas based upon the probability that an area will be vulnerable to SLR impacts at a particular time. The methodology provided in this study is applicable to not only Hawai'i but also all other low-lying coastal areas.

Acknowledgments This project was supported by the U.S. Department of Interior Pacific Islands Climate Change Cooperative Grant No. 6661281. Mahalo Martin Vermeer for providing SLR data.

References

Baker JD, Littnan CL, Johnston DW (2006) Potential effects of sea level rise on the terrestrial habitats of endangered and endemic megafauna in the Northwestern Hawaiian Islands. Endanger Species Res 2:21–30. doi:10.3354/esr002021

Bamber JL, Aspinall WP (2013) An expert judgement assessment of future sea level rise from the ice sheets. Nat Clim Change. doi:10.1038/NCLIMATE1778

Bantilan-Smith M, Bruland GL, MacKenzie RA, Henry AR, Ryder CR (2009) A comparison of the vegetation and soils of natural, restored, and created coastal lowland wetlands in Hawai'i. Wetlands 29:1023–1035. doi:10.1672/08-127.1

Bjerklie DM, Mullaney JR, Stone JR, Skinner BJ, Ramlow MA (2012) Preliminary investigation of the effects of sea-level rise on groundwater levels in New Haven, Connecticut. U.S. Geological Survey Open-File Report 2012–1025, 46 p. http://pubs.usgs.gov/of/2012/1025/

Cooper HM, Chen Q, Fletcher CH, Barbee M (2013a) Assessing vulnerability due to sea-level rise in Maui, Hawai'i using LiDAR remote sensing and GIS. Clim Change 116:547–563. doi:10.1007/s10584-012-0510-9

Cooper HM, Chen Q, Fletcher CH, Barbee M (2013b) Sea-level rise vulnerability mapping for adaptation decisions using LiDAR DEMs. Prog Phys Geogr 37:745–766. doi:10.1177/0309133313496835

Department of Land and Natural Resources (DLNR) (2002) Kanaha pond wildlife sanctuary management plan

Dewberry (2008) LiDAR QAQC report Hawaii TO12: Molokai, Maui, Lanai Islands March 2008. Dewberry, Fairfax, Virginia

Ellison JC (2009) Wetlands of the Pacific Island region. Wetl Ecol Manag 17:169–206. doi:10.1007/s11273-008-9097-3

FGDC (1998) Geospatial positioning accuracy standards, Part 3. National standard for spatial data accuracy. https://www.fgdc.gov/standards/projects/FGDC-standards-projects/accuracy/part3/chapter3. Accessed 19 Aug 2014

Fish MR, Cote IM, Horrocks JA, Mulligan B, Watkinson AR, Jones AR (2008) Construction setback regulations and sea-level rise: mitigating sea turtle nesting beach loss. Ocean Coast Manag 51:330–341. doi:10.1016/j.ocecoaman.2007.09.002

Fletcher C, Rooney J, Barbee M, Lim S-C, Richmond BM (2003) Mapping shoreline change using digital orthophotogeometry on Maui, Hawaii. J Coast Res 38:106–124

Fuentes MMPB, Cinner JE (2010) Using expert opinion to prioritize impacts of climate change on sea turtles' nesting grounds. J Environ Manag 91:2511–2518. doi:10.1016/j.jenvman.2010.07.013

Gesch DB (2009) Analysis of lidar elevation data for improved identification and delineation of lands vulnerable to sea-level rise. J Coast Res SI53:49–58. doi:10.2112/SI53-006.1

Hunt C, De Carlo E (2000) Hydrology and water and sediment quality at James Campbell National Wildlife Refuge near Kahuku, Island of Oahu, Hawaii. http://pubs.usgs.gov/wri/wri99-4171/pdf/wri99-4171.pdf. Accessed 20 July 2014

Intergovernmental Panel on Climate Change (IPCC) (2000) *IPCC special report emission scenarios.* Core writing team Nebojša Nakićenović, Ogunlade Davidson, Gerald Davis, Arnulf Grübler, Tom Kram, Emilio Lebre La Rovere, Bert Metz, Tsuneyuki Morita, William Pepper, Hugh Pitcher, Alexei Sankovski, Priyadarshi Shukla, Robert Swart, Robert Watson, Zhou Dadi, 27 pp. Available online at: https://www.ipcc.ch/pdf/special-reports/spm/sres-en.pdf. Accessed 20 July 2014

Intergovernmental Panel on Climate Change (IPCC) (2007) Climate Change 2007- the physical science basis. In: Solomon S, Qin D, Manning M, Chen Z, Marquis M, Averyt KB, Tignor M, Miller HL (eds) Contribution of working group I to the fourth assessment report of the intergovernmental panel on climate change. Cambridge University Press, Cambridge, United Kingdom. Available online at: http://www.ipcc.ch/publications_and_data/publications_ipcc_fourth_assessment_report_wg1_report_the_physical_science_basis.htm. Accessed 20 July 2014

Intergovernmental Panel on Climate Change (IPCC) (2013) Climate change 2013 the physical science basis. In: Stocker TF, Qin D, Plattner G-K, Tignor MMB, Allen SK, Boschung J, Nauels A, Xia Y, Bex V, Midgley PM (eds) Working group 1 contribution to the fifth assessment report of the intergovernmental panel on climate change. Available online at: http://www.climatechange2013.org/images/report/WG1AR5_Frontmatter_FINAL.pdf. Accessed 18 Aug 2014

Iwamura T, Possingham HP, Chades I, Minton C, Murray NJ, Rogers DI, Treml EA, Fuller RA (2013) Migratory connectivity magnifies consequences of habitat loss from sea-level rise for shorebird populations. Proc R Soc Biol Sci 280:1471–2954. doi:10.1098/rspb.2013.0325

Koshiba S, Besebes M, Soaladaob K, Isechal AI, Victor S, Golbuu Y (2013) Palau's taro fields and mangroves protect the coral reefs by trapping eroded fine sediment. Wetl Ecol Manag 21:157–164. doi:10.1007/s11273-013-9288-4

Krauss KW, Allen JA, Cahoon DR (2003) Differential rates of vertical accretion and elevation change among aerial root types in Micronesian mangrove forests. Estuar Coast Shelf Sci 56:251–259. doi:10.1016/S0272-7714(02)00184-1

Krauss KW, Cahoon DR, Allen JA, Ewel KC, Lynch JC, Cormier N (2010) Surface elevation change and susceptibility of different mangrove zones to sea-level rise on pacific high islands of

Micronesia. Ecosystems 13:129–143. doi:10.1007/s10021-009-9307-8

Mitsova D, Esnard AM, Li Y (2012) Using enhanced dasymetric mapping techniques to improve the spatial accuracy of sea level rise vulnerability assessments. J Coast Conserv 16:355–372. doi:10.1007/s11852-012-0206-3

Moore JG (1987) Subsidence of the Hawaiian Ridge. In: Decker RW, Wright TL, Stauffer PH (ed) Volcanism in Hawai'i, United States Geological Survey Professional Paper, pp 85–100

National Oceanic Atmospheric Administration (NOAA) (2010) Mapping inundation uncertainty. http://csc.noaa.gov/digitalcoast/_/pdf/ElevationMappingConfidence.pdf. Accessed 20 July 2014

Poulter B, Haplin PN (2008) Raster modeling of coastal flooding from sea-level rise. Int J Geogr Inf Sci 22:167–182. doi:10.1080/13658810701371858

Rahmstorf S, Perrette M, Vermeer M (2011) Testing the robustness of semi-empirical sea level projections. Clim Dyn 39:861–875. doi:10.1007/s00382-011-1226-7

Reynolds MH, Berkowits P, Coutrot KN, Krause CM (eds) (2012) Predicting sea-level rise vulnerability of terrestrial habit and wildlife of the Northwestern Hawaiian Islands. U.S. Geological Survey Open-File Report 2012-1182, 139p. http://pubs.usgs.gov/of/2012/1182/. Accessed 20 July 2014

Romine BM, Fletcher CH, Barbee MM, Anderson TR, Frazer LN (2013) Are beach erosion rates and sea-level rise related in Hawaii? Glob Planet Change 108:149–157. doi:10.1016/j.gloplacha.2013.06.009

Rotzoll K, Fletcher C (2012) Assessment of groundwater inundation as consequences of sea level rise. Nat Clim Change 3:477–481. doi:10.1038/nclimate1725

Rotzoll K, El-Kaldi AI, Gingerich SB (2008) Analysis of an unconfined aquifer subject to asynchronous dual-tide propagation. Groundwater 46:239–250. doi:10.1111/j.1745-6584.2007.00412.x

Schaeffer M, Hare W, Rahmstorf S, Vermeer M (2012) Long-term sea-level rise implied by 1.5 C and 2 C warming levels. Nat Clim Change 2:867–870. doi:10.1038/nclimate1584

Slangen ABA, Katsman CA, van de Wal RSW, Vermeersen LLA, Riva REM (2012) Towards regional projections of the twenty-first century sea-level change based on IPCC SRES scenarios. Clim Dyn 38:1191–1201. doi:10.1007/s00382-011-1057-6

Spada G, Bamber JL, Hurkmans RTWL (2013) The gravitationally consistent sea-level fingerprint of future terrestrial ice lost. Geophys Res Lett 40:482–486. doi:10.1029/2012GL053000

Tebaldi C, Strauss BH, Zervas CE (2012) Modelling sea level rise impacts on storm surges along US coasts. Environ Res Lett 7:014032. doi:10.1088/1748-9326/7/1/014032

U.S. Fish and Wildlife Service (2011a) James Campbell National Wildlife Refuge Comprehensive Conservation Plan and Environmental Assessment. http://www.fws.gov/pacific/planning/main/docs/HI-PI/James%20Campbell%20Pearl%20Harbor%20CCP/James%20Campbell%20NWR%20DCCPEA.pdf. Accessed 14 Nov 2014

U.S. Fish and Wildlife Service (2011b) Kealia Pond National Wildlife Refuge Comprehensive Conservation Plan and Environmental Assessment. http://digitalmedia.fws.gov/cdm/singleitem/collection/document/id/453/rec/1. Accessed 14 Nov 2014

U.S. Fish and Wildlife Service (2011c) Recovery plan for Hawaiian waterbird second revision. http://www.fws.gov/pacificislands/CH_Rules/Hawaiian%20Waterbirds%20RP%202nd%20Revision.pdf. Accessed 20 July 2014

Vermeer M, Rahmstorf S (2009) Global sea level linked to global temperature. Proc Natl Acad Sci USA 106:21527–21532. doi:10.1073/pnas.0907765106

Vermeer M, Rahmstorf S, Kemp A, Horton B (2012) On the differences between two semi-empirical sea-level models for the last two millennia. Clim Past Discuss 8:3551–3581. doi:10.5194/cpd-8-3551-2012

Webb EL, Friess DA, Krauss KW, Cahoon DR, Guntenspergen GR, Phelps J (2013) A global Standard for monitoring coastal wetland vulnerability to accelerated sea-level rise. Nat Clim Change 3:458–465. doi:10.1038/nclimate1756

Zhang K (2011) Analysis of nonlinear inundation from sea-level rise using LIDAR data: a case study for South Florida. Clim Change 106:537–565. doi:10.1007/s10584-010-9987-2

Zhang K, Douglas BC, Leatherman SP (2004) Global warming and coastal erosion. Clim Change 64:41–58. doi:10.1023/B:CLIM.0000024690.32682.48

Zhang K, Dittmar J, Ross M, Bergh C (2011) Assessment of sea level rise impacts on human population and real property in the Florida Keys. Clim Change 107:129–146. doi:10.1007/s10584-011-0080-2